

# Unlocked Stripe-order Antiferromagnetism in FeSe under Pressure

P. Wang<sup>1</sup>, S. Sun<sup>1</sup>, Y. Cui<sup>1</sup>, W. Song<sup>1</sup>, T. Li<sup>1</sup>, Rong Yu<sup>1,2\*</sup>, Hechang Lei<sup>1\*</sup>, Weiqiang Yu<sup>1,2\*</sup>

<sup>1</sup>Department of Physics and Beijing Key Laboratory of Opto-electronic Functional Materials & Micro-nano Devices, Renmin University of China, Beijing, 100872

<sup>2</sup>Department of Physics and Astronomy, Shanghai Jiao Tong University, Shanghai 200240, China and Collaborative Innovation Center of Advanced Microstructures, Nanjing 210093, China

\*email: rong.yu@ruc.edu.cn; hlei@ruc.edu.cn; wqyu\_phy@ruc.edu.cn

**Magnetism is essential in understanding unconventional superconductivity. In bulk FeSe, the discovery of a paramagnetic quantum nematic state at ambient pressure, and the emergence of antiferromagnetism and superconductivity with the suppression of the nematic order under pressure, have triggered heated investigation of its intriguing ground-state magnetism. Here we show, by high-pressure <sup>77</sup>Se NMR studies down to 50 mK on FeSe single crystals, that when the nematic order becomes weak, the magnetic structure turns to a novel stripe-order antiferromagnetism with the Fe moments being not locked along any principal axis of crystal. This state breaks the *C*<sub>4</sub> lattice symmetry and undergoes a first-order transition to a paramagnetic phase, in which enhanced stripe-type spin fluctuations are observed in the absence of an orbital order. These results highlight the crucial role of local moments in the magnetism of FeSe and provide vital ingredients for understanding the high-temperature superconductivity in iron chalcogenides and other iron-based superconductors.**

In most iron-based superconductors, superconductivity emerges near an antiferromagnetic (AFM) phase, making it important to study the nature of their magnetism<sup>1,2,3</sup>. For iron pnictides, the magnetic

ground state below  $T_N$  typically has a stripe-type, or  $(\pi, 0)$ , AFM order that breaks the spatial  $C_4$  rotational symmetry<sup>4</sup>. This symmetry is recovered above an orthorhombic-to-tetragonal structural transition at  $T_S \geq T_N$ , leaving space for an electronic nematic phase<sup>5</sup> with a concomitant orbital order below  $T_S$ . The nature of the nematicity and its connection to the antiferromagnetism lead to intense studies, yet still under strong debate<sup>6</sup>. Recent discoveries in the bulk FeSe superconductors<sup>7</sup> make this unsolved issue even more elusive: at ambient pressure, the electronic nematicity shows up below  $T_S \sim 90$  K<sup>8,9</sup>, while a magnetic ordered ground state is absent. Applying a pressure above 1 GPa, however, a magnetic order emerges, and the ordering temperature  $T_N$  increases with pressure<sup>10,11</sup>. Meanwhile,  $T_S$  is substantially suppressed above  $\sim 2$  GPa<sup>12,13</sup>. These seemingly sharp contrasts between FeSe and iron pnictides challenge the existed view of the interplay among the nematicity, orbital ordering and antiferromagnetism, and inspire various theoretical proposals for the magnetism of FeSe<sup>14,15,16,17</sup>. On the experimental side, inelastic neutron scattering measurements suggest the coexistence of stripe and checkerboard spin fluctuations at ambient pressure<sup>18,19</sup>, and high-temperature superconductivity (HTSC) has been observed in both the ambient-pressure nematic and the high-pressure magnetic phases<sup>12,13,20,21</sup>. Therefore, resolving the nematicity and the magnetic structure in FeSe not only helps building up the proper theory on the magnetism of FeSe, but also becomes important in understanding the HTSC observed in bulk FeSe and other iron-based superconductors.

In this work, we present our <sup>77</sup>Se NMR studies on high-quality FeSe single crystals with pressures up to 2.4 GPa and temperatures down to 50 mK. Our main results are summarized in the determined ( $P$ ,  $T$ ) phase diagram in Fig. 1a. From the pressure dependence of the NMR spectral splitting under an in-plane magnetic field, we observe a decrease of the orbital ordering temperature  $T_o$  ( $= T_S$ ) with pressure. However, the stripe-type fluctuations, characterized by the anisotropic  $1/T_1$ , are enhanced

below a weakly pressure dependent temperature  $T^* \sim 100$  K. Above 2 GPa, where the split of the NMR spectra is unable to be detected, we find a novel unlocked stripe-order antiferromagnetic (uS-AFM) phase below  $T_N$ . The thermal transition to this uS-AFM phase is first-order and  $T_N$  increases with pressure. The uS-AFM phase necessarily breaks the lattice  $C_4$  symmetry as the stripe AFM phase in pnictides. But in the former the Fe moments are not locked along any principal axis of crystal, as shown in Fig. 1b. Our discovery of the enhanced stripe-type spin fluctuations above  $T_N$  and the uS-AFM ground state below  $T_N$  under pressure highlights the importance of a local-moment-driven magnetism. Bulk superconductivity is excluded by NMR with pressure above 1.8 GPa; however, the increase of the superconducting transition temperature  $T_C$ , signifies the importance of stripe-type spin fluctuations to high-temperature superconductivity in iron-based superconductors in general (Fig. 1a).

### Orbital ordering

We first determine the evolution of the orbital ordering in the nematic phase under pressure by tracing the NMR line splitting with  $H \parallel a \& b$  (magnetic field applied along the [1 1 0] crystal direction of the tetragonal phase)<sup>22,23</sup>. In Fig. 2a, NMR spectra are shown at  $P = 0.56$  GPa for several selected temperatures, with evidences of orbital order from the NMR line splitting below  $T_o$  in the twinned sample with orthorhombic symmetry. The difference of Knight shifts,  $\Delta^{77}K_{a,b} = |^{77}K_a - ^{77}K_b|$ , where  $^{77}K_a$  and  $^{77}K_b$  are the Knight shifts for  $H \parallel a$  and  $H \parallel b$  respectively, follows a mean-field like temperature dependence, consistent with a second-order phase transition<sup>22</sup>. Similar behaviour of  $\Delta^{77}K_{a,b}$  is observed with pressures up to  $\sim 2$  GPa (Fig. 2b). At  $P = 2.4$  GPa, line splitting is absent above  $T_N$  and cannot be resolved below  $T_N$  (Fig. 3b). As presented in the phase diagram (Fig. 1a),  $T_o$  shows a gradual suppression with pressure.

## Unlocked stripe-order antiferromagnetism

Next we focus on the magnetic properties of the pressurized FeSe. For  $P > 1.34$  GPa, a magnetic phase transition is clearly seen from the peaked feature in  $1/^{77}\text{T}_1T$  (Fig. 4b-c) and the broadening of the NMR spectra upon cooling. Typical spectral data at 2.4 GPa are shown in Fig. 3a-c. Below 30 K, the spectrum with  $H \parallel a\&b$  shifts slightly to the high frequency side, and its full-width-of-half-maximum (FWHM) increases from  $\sim 10$  kHz at  $T = 30$  K to  $\sim 300$  kHz at  $T = 26$  K (Fig. 3a), signaling the magnetic transition. In Fig. 3c, the normalized total spectral weight is drawn as a function of temperature at this pressure. The spectral weight drops steeply by 50% from  $T = 30$  K to 26 K across the magnetic transition, develops a plateau-like feature between 26 K and 18 K, and then decreases slowly upon further cooling because of the RF screening ( $T_C \sim 18$  K under field, see supplementary Fig. S3). The  $1/^{77}\text{T}_1$  shows a sudden drop at 28 K defined as  $T_N$ , coinciding with the middle point of the magnetic transition from the spectral loss. With  $H \parallel c$ , the spectra keep narrow (Fig. 3b), but the total spectral weight starts to lose at 30 K and reaches zero at 26 K (Fig. 3c). No other peaked resonance line is found away from the central frequency with  $H \parallel a\&b$  and  $H \parallel c$  above 2 K, suggesting that the lost spectral weight distributes in a broad lineshape which is undetectable because of low signal-to-noise ratio.

Because of the similar layered structures between FeSe and iron pnictides, we can apply the same analysis to the  $^{77}\text{Se}$  NMR spectra as has been done in  $^{75}\text{As}$  NMR studies for iron pnictides<sup>24,25</sup> (see supplementary S4). This allows us to determine the magnetic structure below  $T_N$ . We show that the change of the spectral weight below  $T_N$  is caused by the formation of a stripe-type AFM order that breaks the  $C_4$  lattice symmetry. The ordered moment on Fe sites is projected as  $(\pm m_{\text{Fe}}^a, \pm m_{\text{Fe}}^b, \pm m_{\text{Fe}}^c)$  to

the principal axes of the orthorhombic structure, and the hyperfine field on the  $^{77}\text{Se}$  is calculated to be  $(H_{in}^a, H_{in}^b, H_{in}^c) = A_{hf}^{ac} (\pm m_{Fe}^c, 0, \pm m_{Fe}^a)$ , where  $A_{hf}^{ac}$  is an off-diagonal hyperfine coupling constant. With nonzero  $m_{Fe}^a$  and  $m_{Fe}^c$ , the spectrum splits for both  $H \parallel a$  and  $H \parallel c$ , but does not split for  $H \parallel b$ . This produces exactly what we have observed: Near the resonant frequency of the paramagnetic phase, the total spectral weight in the ordered phase is zero with  $H \parallel c$ , and 50% with  $H \parallel a&b$  because  $H \parallel a$  and  $H \parallel b$  each occupies 50% volume in twinned orthorhombic domains. It is remarkable that the Fe moments are unlocked to any principal axis of crystal. While in iron pnictides, the Fe moments in the stripe phase are locked in the  $ab$ -plane, evidenced by the 100% spectral weight with  $H \parallel a&b$ <sup>24</sup>.

If the Fe moments of the stripe order AFM are orientated along any of the eight-fold degenerate directions out of the  $ab$  plane, as shown in Fig. 1c, split but peaked NMR lines are expected when the field is applied with  $H \parallel a$  or  $H \parallel c$ . However, we do not find any NMR line away from the center down to 50 mK for  $H \parallel a&b$ . Whereas for  $H \parallel c$ , two split broad NMR lines ( $\sim 300$  kHz) are seen at 50 mK (Fig. 3b), corresponding to  $H_{in}^c \approx 0.48$  T. However, only  $\sim 5\%$  spectra weight is remained, estimated from the central spectrum with  $H \parallel a&b$  at 50 mK. This would suggest the phases with two spin configurations: (i) the moments are partially unlocked and centered around the eight-fold degenerate directions with a broad distribution (Fig. 1c); (ii) the orientation of Fe moments in each magnetic domain is almost fully unlocked and broadly distributed by picking its own direction on a spherical surface as shown in Fig. 1c. The second one is the majority phase occupying  $\sim 95\%$  volume. In both cases, weak incommensurability may further help to stabilize the broad spectrum. Our simulations suggest that the majority phase is also consistent with the lineshape with  $H \parallel b$  (see supplementary S5). As shown in Fig. 3a, the spectra with  $H \parallel a&b$  at 2 K (same for 50 mK) is well fit by the fully unlocked

stripe order with parameters  $|H_{in}| = 0.95$  T and a misaligned angle  $\delta \approx 1.1^\circ$  between the external field and the  $b$ -axis.

The above analyses on the NMR spectra already allow us to rule out various proposed magnetic structures, including, but not limited to, spin glasses, checkerboard  $(\pi, \pi)$  spin orders, double-Q stripe phases, incommensurate SDW or spiral orders with propagating wave vectors far away from  $(\pi, 0)$ ,  $(\pi/2, \pi/2)$  double stripes, and staggered dimer/trimmer spin patterns. These magnetic orders either cannot account for the spectral weight loss or fail to generate the broad lineshape with the two field configurations (see supplementary S6).

The uS-AFM order is very different from the stripe order in iron pnictides in which the Fe moments are locked along the crystal  $a$ -axis. In iron pnictides, the spin-anisotropic energy, from the combined effect of orbital ordering and spin-orbit coupling, is less than 0.2 meV.<sup>26</sup> Though the spin-orbit coupling may be slightly increased in FeSe<sup>27</sup>, such a small spin-anisotropic energy may not be strong enough to lock the spins when  $T_o$  is low at high pressures. To our best knowledge, this uS-AFM in FeSe is discovered for the first time in iron-based superconductors, and gives a second example of unlocked magnetic phases besides MnSi<sup>28,29,30</sup>. With the absence of spin locking, FeSe may supply as another potential functional material for spin manipulations.

We have also examined the magnetic transition across  $T_N$  from the temperature scan of the  $1/^{77}T_1T$ , as shown in Fig. 4a-c. For pressures from 1.34 GPa to 1.86 GPa, the  $1/^{77}T_1T$  has a clear divergence at  $T_N$ , suggesting a second-order magnetic transition. Surprisingly, the divergence is completely absent at  $T_N$  under higher pressures (above 2 GPa), directly evidencing a strong first-order transition with no critical fluctuations. The first-order nature of the transition is further supported by the hysteresis near  $T_N$ , with a 1.5 K shift in the temperature dependence of the integrated spectral weight with  $H \parallel c$

between cooling and warming at 0.1 K/min (Fig. 3c). This may imply that the magnetic transition is coupled to a structural one which breaks the  $C_4$  lattice symmetry, as will be discussed.

### Stripe-type spin fluctuations

We are now in a position to discuss the spin fluctuations above  $T_N$  from the  $1/^{77}T_1$  data. Fig. 3d shows the  $(1/^{77}T_1)_{H \parallel a\&b}$  and  $(1/^{77}T_1)_{H \parallel c}$  below 200 K under two pressures,  $P = 1.34$  GPa and 2.4 GPa. In the inset, the anisotropy factor  $R = (1/^{77}T_1)_{H \parallel a\&b} / (1/^{77}T_1)_{H \parallel c}$  at these two pressures are also presented from 100 K down to 40 K, where  $R \approx 1.5$  holds. This value of  $R$  is an indication of stripe-type spin fluctuations (see supplementary S4), persisting to the highest pressure we measured, in consistence with the ground state magnetism we presented. The possibility of checkerboard-type spin fluctuations, which has  $R = 0.5$  (see Fig. 3d inset), is ruled out as candidate magnetism. Remarkably, as shown in Fig. 4a-c, the high-temperature  $1/^{77}T_1T$  has a shallow minimum at  $T^* \sim 100$  K under all pressures, and shows an upturn upon further cooling. This indicates the existence of a characteristic temperature,  $T^*$ , below which the stripe fluctuations are enhanced as shown in the phase diagram (Fig. 1a).

### Discussions and conclusions

In the uS-AFM phase of FeSe, the 50% spectral loss with  $H \parallel a\&b$  evidences the existence of twinned magnetic domains, each breaks the lattice  $C_4$  symmetry with either  $a \parallel H$  or  $b \parallel H$ . As a result, the magnetic transition is necessarily coupled to a tetragonal-to-orthorhombic structural transition, which may take place exactly at or slightly above  $T_N$ , promoted by spin-phonon coupling<sup>31,32</sup>, which may take place exactly at or slightly above  $T_N$ . This scenario is compatible with our observed

first-order magnetic transition and the persistence of the orthorhombic structure shown in the high-pressure XRD data<sup>33</sup>.

Since the nematic order naturally couples to the orbital order, an interesting question is then raised: whether the stripe AFM order is driven by orbital order. Our data provide unambiguous evidence that this is not the case. First, in the pressure range where both  $T_N$  and  $T_o$  are observed, it would be difficult to understand the suppression of  $T_o$  but the simultaneous enhancement of  $T_N$  if both the magnetic and structural transitions originate from the orbital order. Second, in the full range of pressure we have measured, enhanced stripe-type fluctuations exist up to  $T^* \sim 100$  K. Note that  $T^* > T_o$  and  $T_N$ , this explicitly shows that the spin fluctuations are not driven by orbital order as well. Moreover, the Fermi surface remains small and varies weakly with pressure in the AFM phase above 1.4 GPa, as shown in a recent quantum oscillation study<sup>34</sup>. This implies that the enhancement of  $T_N$  under pressure is incompatible with the itinerant magnetism based on the orbital physics. Instead, our results reveal that localized magnetic moments play an essential role for physical properties of FeSe, as proposed by several theories<sup>14,15,16,17</sup>.

Finally, we address the implications of our data to superconductivity. The  $T_C$ , shown in Fig. 1a, is independently determined by our *ac* inductance measurements (see supplementary S3). Below 1 GPa, the onset of  $T_C$  is also shown by a kinked feature in the  $1/T_1T$  upon cooling (Fig. 4a), which signals bulk superconductivity. Above 1.5 GPa, while both  $T_C$  and  $T_N$  increase with pressures, the  $1/T_1T$  drops smoothly and does not show any kinked feature across  $T_C$ . This indicates a very low volume fraction of the superconducting phase, thus ruling out bulk superconductivity. It is most likely that superconductivity resides in nanostructures, such as magnetic domain walls. This may draw a connection to single-layer FeSe, which also exhibits nanoscale superconductivity<sup>35</sup>.



Coincident with the evolution of  $T_C$ , the  $1/T_1T$  at 100 K also increases with pressure (Fig. 4d), consistent with earlier NMR results on polycrystals<sup>10</sup>. More importantly, our analysis on the anisotropy factor specifies that dominant spin fluctuations in FeSe are the stripe type, as is in iron pnictides. Therefore, stripe magnetism seems to be universal in all iron-based superconductors and play an essential role for their pairing<sup>36,37</sup>. Our pressure enhanced stripe-type fluctuations may help to understand the significant increase of  $T_C$  at 6 GPa in FeSe, when the competing long-range order antiferromagnetism is suppressed<sup>13</sup>.

In summary, we report the first spectroscopic evidence for the evolution of the orbital ordering in bulk FeSe under pressure, and discover a novel unlocked stripe-order antiferromagnetism. Our results indicate the local moment, but not the orbital physics, origin of stripe-order antiferromagnetism in the iron-based superconductors. Moreover, we reveal the persistent stripe-type spin fluctuations over a wide range of temperature and pressure, which should help to understand the emergent high-temperature superconductivity. These findings deepen our understanding of the interplay between magnetism and superconductivity not only in FeSe, but also in other iron-based superconductors.

## Methods

The FeSe single crystals were synthesized by a temperature-gradient-assisted flux method (details in supplementary S1) for 30 days. The tetragonal FeSe crystals with the (0 0 1) orientation is grown with sizes up to  $4 \times 3 \times 0.03$  mm<sup>3</sup>. The X-ray, magnetization and resistivity data are shown in Fig. S1 and S2. The crystal  $a$ ,  $b$ , and  $c$ -axis were determined by X-ray diffraction. The samples are cut into squares with edges along the tetragonal [1 1 0] direction for high pressure NMR measurements. The NMR measurements were performed with two field configurations under a 10.3 T magnetic field.

Daphne oil was used as the pressure medium, and the pressure was determined by  $\text{Cu}_2\text{O}$  NQR resonance frequency at low temperatures<sup>38</sup>. For pressure above 2 GPa, the pressure cell was heated to 80 °C when applying pressure in order to get better hydrostaticity<sup>39</sup>. Standard spin-echo and CPMG techniques were used for data accumulation to optimize the signal-to-noise ratio. The FWHM of  $^{77}\text{Se}$  spectra is  $\sim 4$  kHz at 100 K at all pressures, indicating high sample quality and pressure homogeneity. The spin-lattice relaxation rates were measured with the inversion-recovery method. Below the onset temperature of the orbital order, the spin-lattice relaxation rates of the high-frequency peak and the low-frequency one show similar behaviours, and only the former one is presented.

## References

1. Paglione, J. & Greene, R. L. High-temperature superconductivity in iron-based materials. *Nature Phys.* **6**, 645-658 (2010).
2. Stewart, G. R. Superconductivity in iron compounds. *Rev. Mod. Phys.* **83**, 1589 (2011).
3. Dai, P. Antiferromagnetic order and spin dynamics in iron-based superconductors. *Rev. Mod. Phys.* **87**, 855 (2015).
4. De la Cruz, C. *et al.* Magnetic order close to superconductivity in the iron-based layered  $\text{LaO}_{1-x}\text{F}_x\text{FeAs}$  systems. *Nature* **453**, 899-902 (2008).
5. Chu, J-H. *et al.* In-Plane Resistivity Anisotropy in an Underdoped Iron Arsenide Superconductor. *Science* **329**, 824-826 (2010).
6. Fernandes, R. M., Chubukov, A. V. & Schmalian, J. What drives nematic order in iron-based superconductors? *Nature Phys.* **10**, 97-104 (2014).
7. Hsu, F. C. *et al.* Superconductivity in the PbO-type structure  $\alpha\text{-FeSe}$ . *Proc. Natl. Acad. Sci.* **105**, 14262-14264 (2008).

8. McQueen, T. M. *et al.* Tetragonal-to-Orthorhombic Structural Phase Transition at 90 K in the Superconductor Fe<sub>1.01</sub>Se. *Phys. Rev. Lett.* **103**, 057002 (2009).
9. Shimojima, T. *et al.* Lifting of xz/yz orbital degeneracy at the structural transition in detwinned FeSe. *Phys. Rev. B* **90**, 121111(R) (2014).
10. Imai, T., Ahilan, K., Ning, F. L., McQueen, T. M. & Cava, R. J. Why Does Undoped FeSe Become a High-T<sub>c</sub> Superconductor under Pressure? *Phys. Rev. Lett.* **102**, 177005 (2009).
11. Bendele, M. *et al.* Pressure Induced Static Magnetic Order in Superconducting FeSe<sub>1-x</sub>. *Phys. Rev. Lett.* **104**, 087003 (2010).
12. Terashima, T. *et al.* Pressure-Induced Antiferromagnetic Transition and Phase Diagram in FeSe. *J. Phys. Soc. Jpn.* **84**, 063701 (2015).
13. Sun, J. P. *et al.* Dome-shaped magnetic order competing with high-temperature superconductivity at high pressures in FeSe. Preprint at <http://arxiv.org/abs/1512.06951> (2015).
14. Yu, R. & Si, Q. M. Antiferroquadrupolar and Ising-Nematic Orders of a Frustrated Bilinear-Biquadratic Heisenberg Model and Implications for the Magnetism of FeSe. *Phys. Rev. Lett.* **115**, 116401 (2015).
15. Wang, F., Kivelson, S. A. & Lee, D-H. Nematicity and quantum paramagnetism in FeSe. *Nature Phys.* **11**, 959-963 (2015).
16. Glasbrenner, J. K. *et al.* Effect of magnetic frustration on nematicity and superconductivity in iron chalcogenides. *Nature Phys.* **11**, 953-958 (2015).
17. Liu, K., Lu, Z-Y & Xiang, T. Nematic antiferromagnetic states in bulk FeSe. Preprint at <http://arxiv.org/abs/1510.07447> (2015).
18. Rahn, M. C., Ewings R. A., Sedlmaier S. J., Clarke, S. J. & Boothroyd, A. T. Strong ( $\pi,0$ ) spin

- fluctuations in  $\beta$ -FeSe observed by neutron spectroscopy. *Phys. Rev B* **91**, 180501(R) (2015).
19. Wang, Q. S. *et al.* Magnetic ground state of FeSe. Preprint at <http://arxiv.org/abs/1511.02485> (2015).
20. GarBarino, G. *et al.* High-temperature superconductivity ( $T_c$  onset at 34 K) in the high-pressure orthorhombic phase of FeSe. *Europhys. Lett.* **86**, 27001 (2009).
21. Medvedev, S. *et al.* Electronic and magnetic phase diagram of  $\beta$ -Fe<sub>1.01</sub>Se with superconductivity at 36.7 K under pressure. *Nature Mater.* **8**, 630-633 (2009).
22. Baek, S-H. *et al.* Orbital-driven nematicity in FeSe. *Nature Mater.* **10**, 210-214 (2015).
23. Böhmer, A. E. *et al.* Origin of the Tetragonal-to-Orthorhombic Phase Transition in FeSe: A Combined Thermodynamic and NMR Study of Nematicity. *Phys. Rev. Lett.* **114**, 027001 (2015).
24. Kitagawa, K., Katayama, N., Ohgushi, K., Yoshida, M. & Takigawa, M. Commensurate Itinerant Antiferromagnetism in BaFe<sub>2</sub>As<sub>2</sub>: <sup>75</sup>As-NMR Studies on a Self-Flux Grown Single Crystal. *J. Phys. Soc. Jpn.* **77**, 114709 (2008).
25. Kitagawa, S. *et al.* Stripe antiferromagnetic correlations in LaFeAsO<sub>1-x</sub>F<sub>x</sub> probed by <sup>75</sup>As NMR. *Phys. Rev. B* **81**, 212502 (2011).
26. Lee, J. H., Jang, H. M. & Choi, H. J. Effects of spin-orbit interaction on the magnetic and electronic structure of antiferromagnetic LaFeAsO. Preprint at <http://arxiv.org/abs/1008.1035> (2010).
27. Borisenko, S. V. Direct observation of spin-orbit coupling in iron-based superconductors. *Nature Phys.* (2015), doi:10.1038/nphys3594.
28. Pfleiderer, C. *et al.* Partial order in the non-Fermi-liquid phase of MnSi. *Nature* **427**, 227-231 (2004).
29. Yu, W. *et al.* Phase Inhomogeneity of the Itinerant Ferromagnet MnSi at High Pressures. *Phys. Rev.*

- Lett.* **92**, 086403 (2004).
30. Uemura, Y. J. *et al.* Phase separation and suppression of critical dynamics at quantum phase transitions of MnSi and  $(\text{Sr}_{1-x}\text{Ca}_x)\text{RuO}_3$ . *Nature Phys.* **3**, 29-35 (2007).
31. Ye, Q. Q., Liu, K. & Lu, Z. Y. Influence of spin-phonon coupling on antiferromagnetic spin fluctuations in FeSe under pressure: First-principles calculations with van der Waals corrections. *Phys. Rev. B* **88**, 205130 (2013).
32. Lischner, J., Bazhiron, T., MacDonald, A. H., Cohen, M. L. & Louie, S. G. First-principles theory of electron-spin fluctuation coupling and superconducting instabilities in iron selenide. *Phys. Rev. B* **91**, 020502(R) (2015).
33. Margadonna, S. *et al.* Pressure evolution of the low-temperature crystal structure and bonding of the superconductor FeSe ( $T_c = 37$  K). *Phys. Rev. B* **89**, 064506 (2009).
34. Terashima, T. *et al.* Fermi surface reconstruction in FeSe under high pressure. Preprint at <http://arxiv.org/abs/1510.01840> (2015).
35. Wang, Q. Y. *et al.* Interface-Induced High-Temperature Superconductivity in Single Unit-Cell FeSe Films on  $\text{SrTiO}_3$ . *Chin. Phys. Lett.* **29**, 037402 (2012).
36. Essenberger, F. *et al.* Ab-initio theory of Iron based superconductors. Preprint at <http://arxiv.org/abs/1411.2121> (2014).
37. Watashige, T. *et al.* Evidence for Time-Reversal Symmetry Breaking of the Superconducting State near Twin-Boundary Interfaces in FeSe Revealed by Scanning Tunneling Spectroscopy. *Phys. Rev. X* **5**, 031022 (2015).
38. Reyes, A. P., Ahrens, E. T., Heffner R. H., Hammel, P. C. & Thompson J. D. Cuprous oxide manometer for high-pressure magnetic resonance experiments. *Rev. Sci. Instrum.* **63**, 3120 (1992).

39. Yokogawa, K., Murata, K., Yoshino, H. & Aoyama S. Solidification of High-Pressure Medium Daphne 7373. *Jpn. J. Appl. Phys.* **46**, 2626-3639 (2007).

### **Acknowledgement**

We acknowledge encouraging discussions with Zhong-Yi Lu, Dong-Hai Lee, Tao Xiang, Kai Liu, Fa Wang, and Qimiao Si. Work at Renmin University of China is supported by the National Science Foundation of China (NSFC) (Grant Nos. 11222433, 11374361, 11374364 and 11574394), the Ministry of Science and Technology of China (973 Projects: 2012CB921701), and the Fundamental Research Funds for the Central Universities and the Research Funds of Remnin University of China (Grant Nos. 14XNLF08, 15XNLQ07 and 15XNLF06).

### **Author Contributions**

S. S. and H. L. synthesized the signal crystals and performed X-ray diffraction, magnetization and resistivity measurements. W. Y. designed the NMR measurements, and P. W., Y. C., W. S. and T. L. performed all NMR measurements. P. W. did most data analysis. W. Y., R. Y., and H. L. wrote the manuscript.

### **Competing financial interests**

The authors declare no competing financial interests.

### **Additional information**

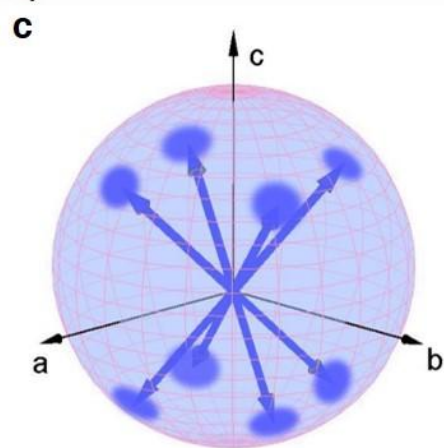
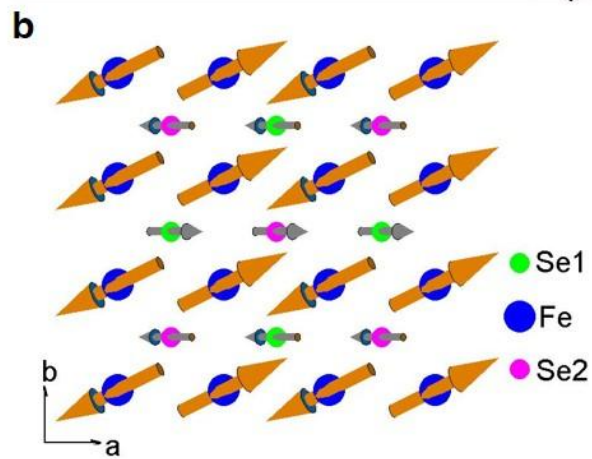
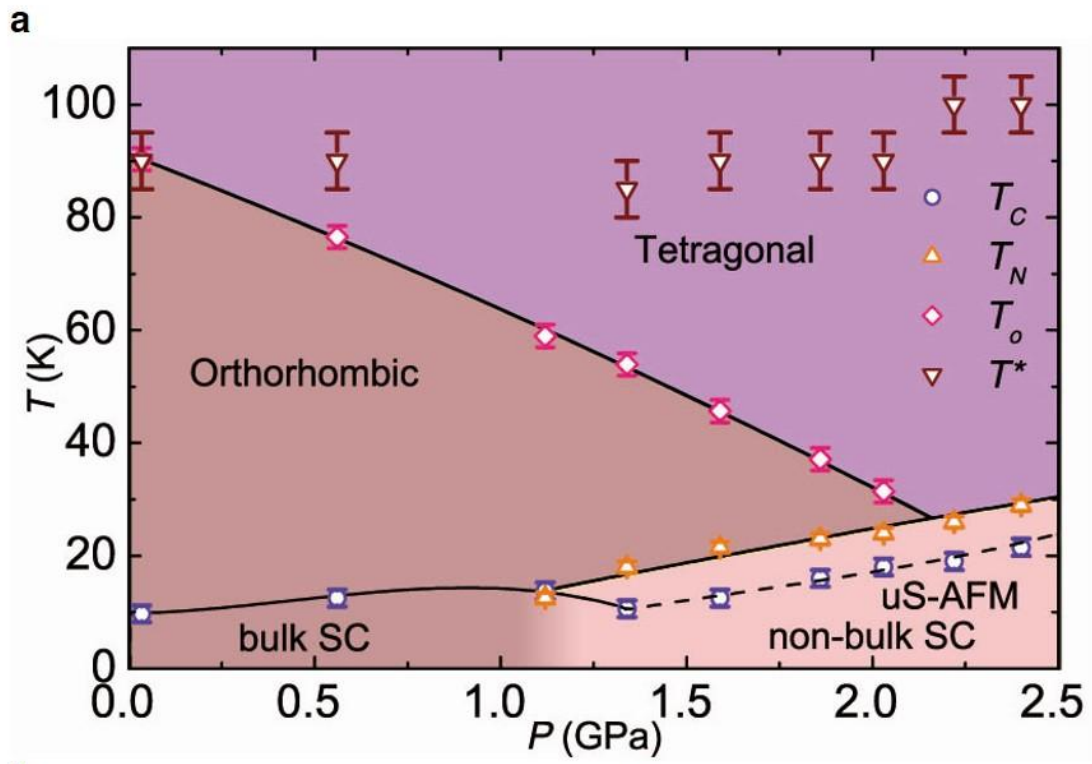
Supplementary information is available in the online version of the paper.

**Figure 1 | The ( $P$ ,  $T$ ) phase diagram of bulk FeSe and the illustrations for the unlocked stripe-order. a,** The phase diagram with the orbital order transition temperature  $T_o$ , the unlocked stripe-order antiferromagnetism (uS-AFM) transition temperature  $T_N$ , and the superconducting transition temperature  $T_C$ . The  $T^*$  is a temperature below which the stripe-type spin fluctuations are enhanced. **b,** An illustration of the uS-AFM with Fe moments pointing out of the  $ab$ -plane and the resulting hyperfine field on the  $^{77}\text{Se}$  nuclei in the  $ac$ -plane. **c,** A sketch illustrating the distributed Fe moment orientations with an eight-fold degeneracy in a partially unlocked stripe-order antiferromagnetism.

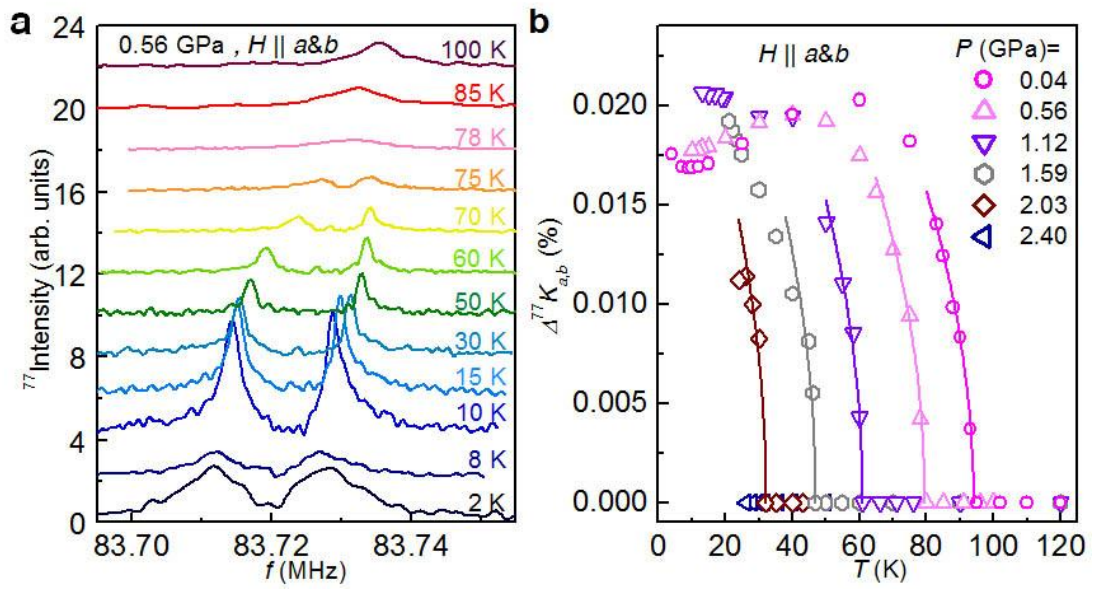
**Figure 2 | The orbital ordering of bulk FeSe under pressure. a,** The characteristic  $^{77}\text{Se}$  spectra showing the orbital ordering by the line splitting with  $H \parallel a\&b$  at  $P = 0.56$  GPa. **b,** The difference of Knight shifts,  $\Delta^{77}K_{a,b} = |^{77}K_a - ^{77}K_b|$ , measured as a function of temperature at various pressures. The solid lines are the fits to a mean-field function  $\Delta^{77}K_{a,b} \sim 1/(T_o - T)^{1/2}$ .

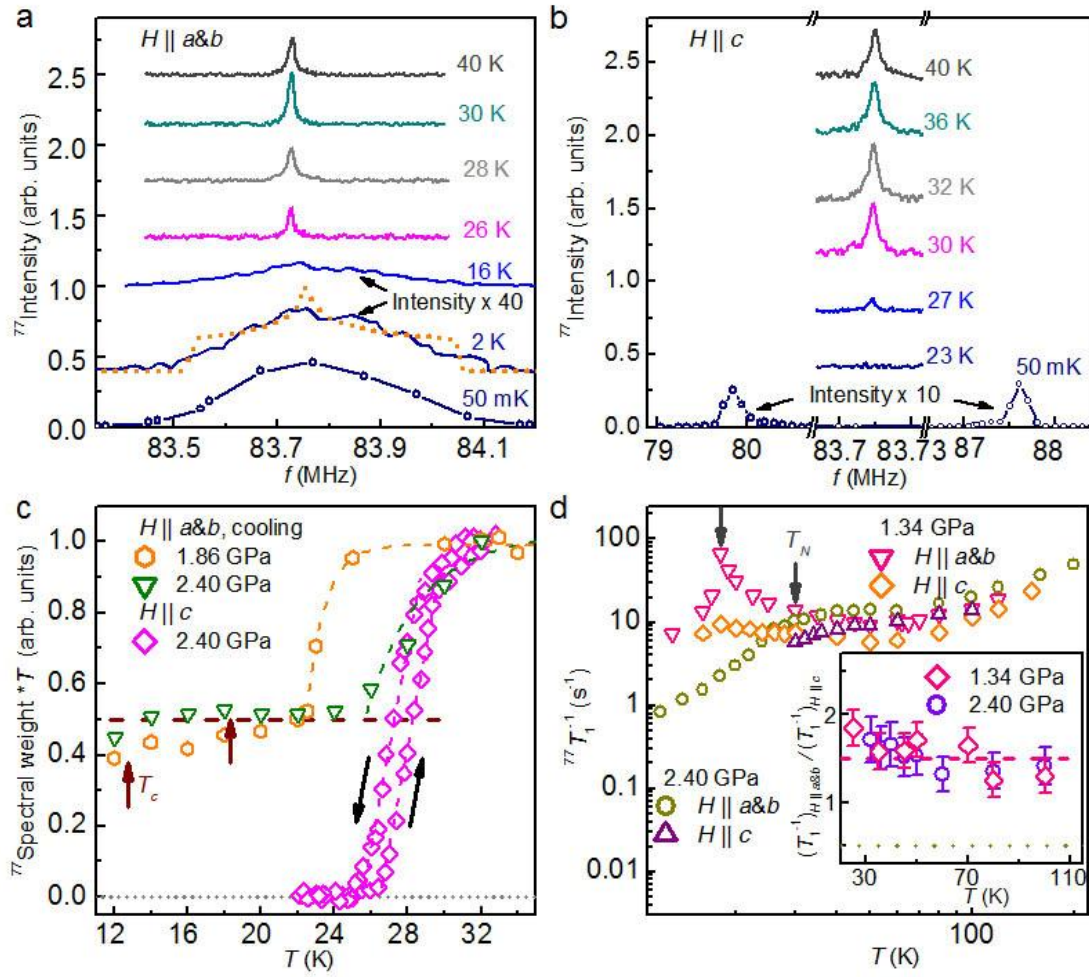
**Figure 3 | Evidences of unlocked stripe-type antiferromagnetism of bulk FeSe at high pressures. a** and **b,** The NMR spectra with  $H \parallel a\&b$  and  $H \parallel c$  at  $P = 2.4$  GPa. The dotted line in (a) is a fit to the spectra ( $T = 2$  K) by the fully uS-AFM with field applied  $1.1^\circ$  off the  $b$ -axis. **c,** The normalized total spectral weight as a function of temperature at high pressures. The dashed horizontal line is an eye guide to the 50% spectral weight. **d,** The spin-lattice relaxation rate  $1/^{77}T_1$  for two field configurations and at  $P = 1.34$  and  $2.4$  GPa. Inset: the anisotropy factor  $R = (1/^{77}T_1)_{H \parallel a\&b} / (1/^{77}T_1)_{H \parallel c}$  as a function of temperature. The dashed and dotted horizontal lines are the theoretical values for the stripe-type ( $R = 1.5$ ) and for the checkerboard-type ( $R = 0.5$ ) spin fluctuations.

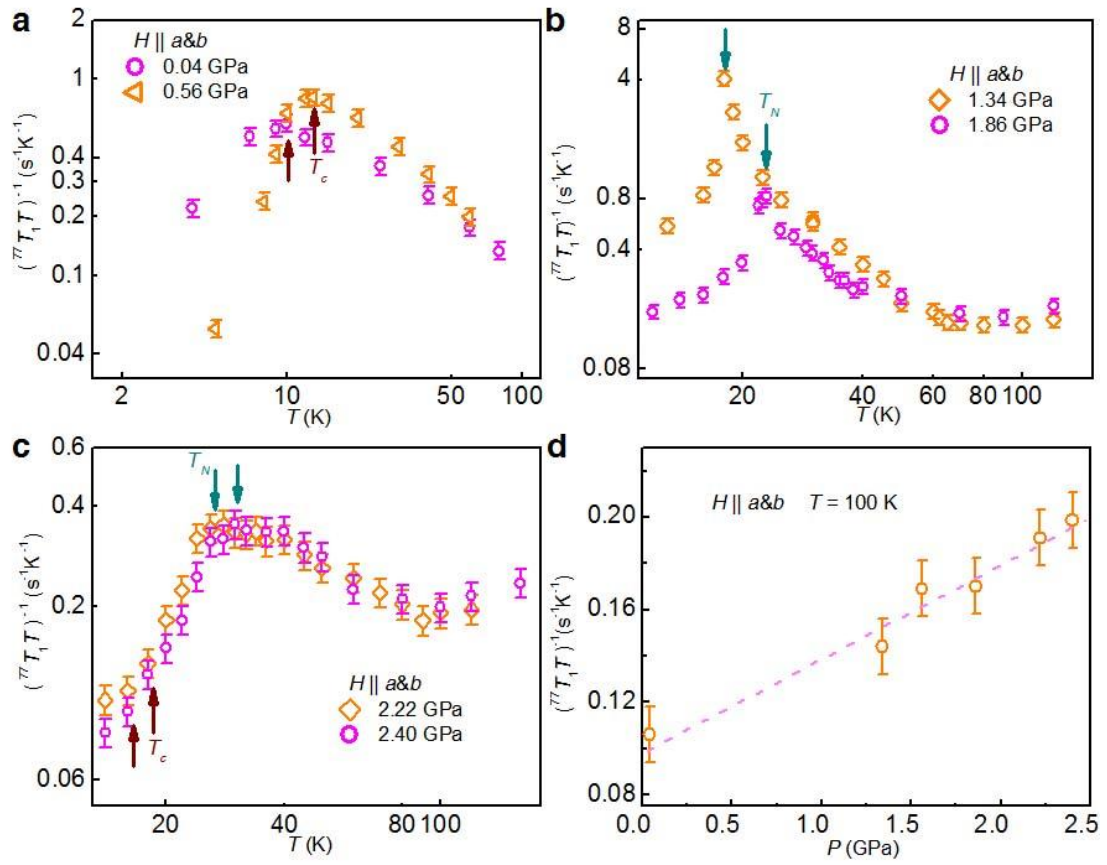
**Figure 4 | The  $^{77}\text{Se}$  spin-lattice relaxation rate. a, b, and c,** The spin-lattice relaxation rate divided by temperature ( $1/^{77}T_1 T$ ) with  $H \parallel a\&b$  at typical pressures. The up arrows denote the  $T_C$  determined by *in situ*  $ac$  inductance measurements, and the down arrows denote the  $T_N$ . **d,** The plot of  $1/^{77}T_1 T$  at 100 K as a function of pressure.











# Unlocked Stripe-order Antiferromagnetism in FeSe under Pressure

P. Wang<sup>1</sup>, S. Sun<sup>1</sup>, Y. Cui<sup>1</sup>, W. Song<sup>1</sup>, T. Li<sup>1</sup>, Rong Yu<sup>1,2\*</sup>, Hechang Lei<sup>1\*</sup>, Weiqiang Yu<sup>1,2\*</sup>

<sup>1</sup>Department of Physics and Beijing Key Laboratory of Opto-electronic Functional Materials & Micro-nano Devices, Renmin University of China, Beijing, 100872

<sup>2</sup>Department of Physics and Astronomy, Shanghai Jiao Tong University, Shanghai 200240, China and Collaborative Innovation Center of Advanced Microstructures, Nanjing 210093, China

\*email: rong.yu@ruc.edu.cn; hlei@ruc.edu.cn; wqyu\_phy@ruc.edu.cn

## Supplemental Materials

### S1. Crystal Growth of $\beta$ -FeSe single crystals by a temperature-gradient assisted flux method

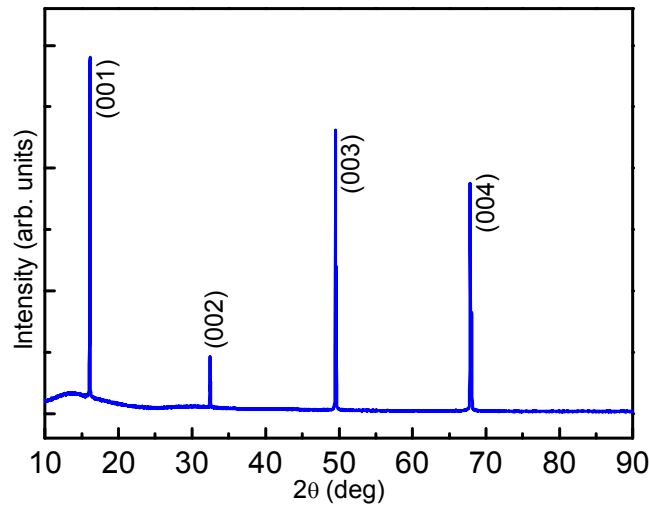


**Figure S1.** XRD pattern of a  $\beta$ -FeSe single crystal, showing (0 0 1)-oriented tetragonal phase.

The iron and selenium powder were mixed by the ratio Fe : Se = 1 : 1 with eutectic flux by the ratio  $\text{AlCl}_3$  :  $\text{NaCl}$  = 0.52 : 0.48, loaded in an ampoule, evacuated down to  $10^{-5}$  bar, and then sealed. The ampoule was heated with a uniform temperature gradient where temperature changes from 690 K to 620 K in a horizontal furnace. After 30 days of growth, the furnace was shut down and the ampoule was cooled naturally. After rinsed in distilled water and alcohol, tetragonal crystals with typical sizes of  $\sim 4 \times 3 \times 0.03 \text{ mm}^3$  were obtained. X-ray diffraction (XRD) measurement of single crystals was

performed on a Bruker D8 X-ray machine with Cu  $K_\alpha$  radiation ( $\lambda = 0.15418$  nm) at room temperature (Fig. S1). All crystals exhibit a (0 0 1)-oriented tetragonal phase, and the natural cleavage edge is confirmed to be along the tetragonal [1 0 0] direction.

## S2. Electric transport and magnetization measurements

The electric transport and dc magnetization measurements were performed in a Quantum Design PPMS-14T. The magnetization (Fig. S2a) was measured with  $H \parallel c$  under a 10 Oe field by the field-cooling (FC) and zero-field-cooling (ZFC) modes. The resistivity was measured by the standard four-probe method. The onset superconducting transition temperature  $T_C$  is  $\sim 8.79$  K, and the structural transition temperature  $T_S$  is  $\sim 89$  K shown by a small kink on the resistivity (Fig. S2b).

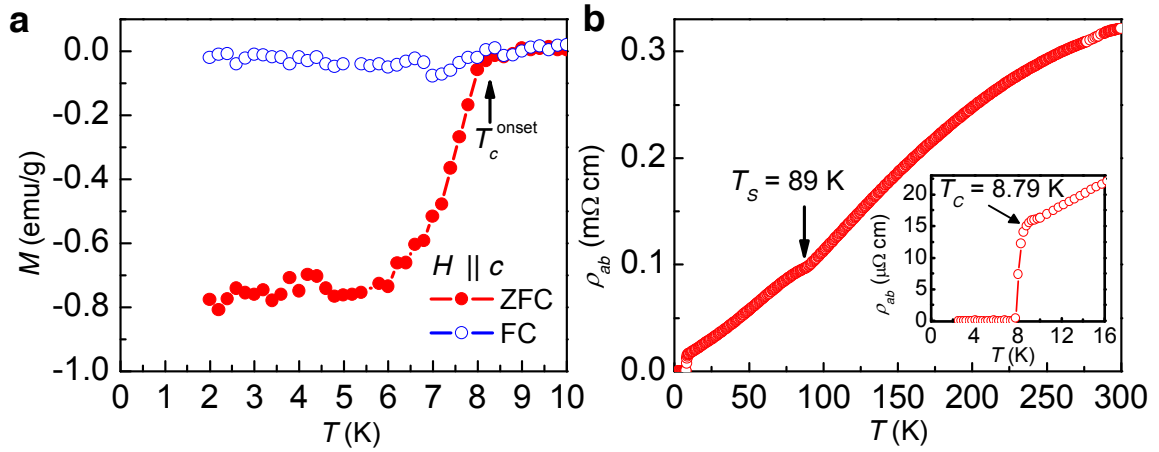


**Figure S2.** **a**, Temperature dependence of magnetization at  $H = 10$  Oe by ZFC and FC modes for a  $\beta$ -FeSe single crystal. The arrow marks the onset  $T_C \sim 8.19$  K. **b**, Temperature dependence of the in-plane resistivity  $\rho_{ab}(T)$  at zero field. Inset: The enlarged view of  $\rho_{ab}(T)$  at the low-temperature region.

## S3. $T_C$ of the FeSe NMR crystal measured *in situ* under pressure

The resonant frequency  $f$  of the NMR RLC circuit is susceptible to the sample in the inductance coil. The superconducting sample has a large diamagnetization effect, and thus reduces the coil

inductance and lifts up the resonance frequency when cooling below  $T_C$ . The  $T_C$  of the NMR sample is determined by the sudden increase of  $f$ . In Fig. S3a-b, we show the change of  $f$  with temperature under various pressures at a warming rate of 0.1 K/min, measured at zero field and under the NMR field.

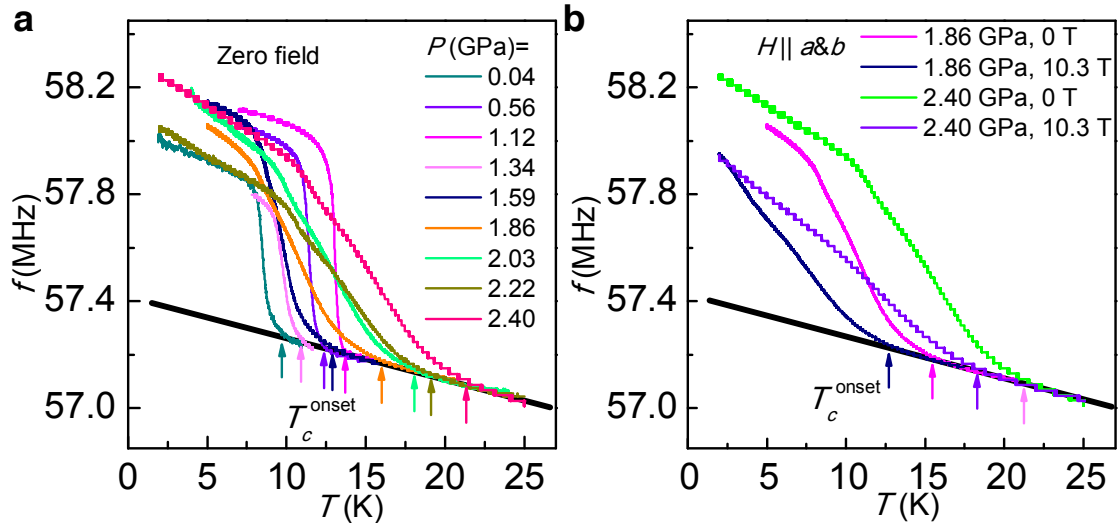


**Figure S3.** The resonance frequency  $f$  of the NMR circuit measured (a) at zero field, and (b) under a 10.3 T in-plane field. The onset  $T_C$  is indicated by the arrows. The black line is a guide of background.

#### S4. Anisotropy of the $^{77}\text{Se}$ hyperfine fields and the $1/T_1$

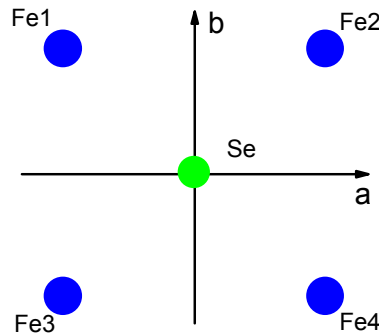


**Figure S4.** The projection of one FeSe plaquette with four Fe atoms and one Se atom. Se sites are located alternatively above and below the Fe plane.

Because of the similar layered structures of FeSe- and FeAs-based superconductors, the same symmetry analysis<sup>1,2</sup> can be performed on the hyperfine field and the spin-lattice relaxation rate. In FeSe, each Se site has four Fe neighbors but locating out of the Fe plane (Fig. S4). The total hyperfine

field on the  $^{77}\text{Se}$  site arising from Fe magnetic moments is written in the following form,

$$\mathbf{H}_{in} = \sum_{i=1}^4 \mathbf{A}_{hf}^i \cdot \mathbf{m}_{\text{Fe}}^i, \quad (\text{A1})$$

where  $\mathbf{m}_{\text{Fe}}^i$  is the ordered magnetic moment of the  $i$ -th Fe atom ( $i = 1, 2, 3, 4$ ), and  $\mathbf{A}_{\text{Fe}}^i$  is a hyperfine coupling tensor between the  $^{77}\text{Se}$  nucleus and the  $i$ -th Fe moment.

We first express the  $\mathbf{A}_{\text{Fe}}^1$  and  $\mathbf{m}_{\text{Fe}}^1$  as

$$\mathbf{A}_{hf}^1 = \begin{bmatrix} A_{hf}^{aa} & A_{hf}^{ab} & A_{hf}^{ac} \\ A_{hf}^{ba} & A_{hf}^{bb} & A_{hf}^{bc} \\ A_{hf}^{ca} & A_{hf}^{cb} & A_{hf}^{cc} \end{bmatrix} \text{ and } \mathbf{m}_{\text{Fe}}^1 = \begin{bmatrix} m_{\text{Fe}}^a \\ m_{\text{Fe}}^b \\ m_{\text{Fe}}^c \end{bmatrix}, \quad (\text{A2})$$

where  $a$ ,  $b$  and  $c$  are the three crystal axes of FeSe in the orthorhombic phase. Applying mirror symmetry analysis, the hyperfine coupling tensors related to the other three Fe atoms follow as

$$\begin{aligned} \mathbf{A}_{hf}^2 &= \begin{bmatrix} A_{hf}^{aa} & -A_{hf}^{ab} & -A_{hf}^{ac} \\ -A_{hf}^{ba} & A_{hf}^{bb} & A_{hf}^{bc} \\ -A_{hf}^{ca} & A_{hf}^{cb} & A_{hf}^{cc} \end{bmatrix}, \quad \mathbf{A}_{hf}^3 = \begin{bmatrix} A_{hf}^{aa} & -A_{hf}^{ab} & A_{hf}^{ac} \\ -A_{hf}^{ba} & A_{hf}^{bb} & -A_{hf}^{bc} \\ A_{hf}^{ca} & -A_{hf}^{cb} & A_{hf}^{cc} \end{bmatrix}, \text{ and} \\ \mathbf{A}_{hf}^4 &= \begin{bmatrix} A_{hf}^{aa} & A_{hf}^{ab} & -A_{hf}^{ac} \\ A_{hf}^{ba} & A_{hf}^{bb} & -A_{hf}^{bc} \\ -A_{hf}^{ca} & -A_{hf}^{cb} & A_{hf}^{cc} \end{bmatrix}. \end{aligned} \quad (\text{A3})$$

Next we consider two magnetic orders with stripe  $(\pi, 0)$  and checkerboard  $(\pi, \pi)$  patterns. The stripe pattern is defined as

$$\mathbf{m}_{\text{Fe}}^1 = -\mathbf{m}_{\text{Fe}}^2 = \mathbf{m}_{\text{Fe}}^3 = -\mathbf{m}_{\text{Fe}}^4. \quad (\text{A4})$$

The internal hyperfine field on the  $^{77}\text{Se}$  sites is obtained as

$$\mathbf{H}_{in} = (\mathbf{A}_{hf}^1 - \mathbf{A}_{hf}^2 + \mathbf{A}_{hf}^3 - \mathbf{A}_{hf}^4) \cdot \mathbf{m}_{\text{Fe}}^1 = 4A_{hf}^{ac} \begin{bmatrix} m_{\text{Fe}}^c \\ 0 \\ m_{\text{Fe}}^a \end{bmatrix}. \quad (\text{A5})$$

On the other hand, the checkerboard pattern follows

$$\mathbf{m}_{\text{Fe}}^1 = -\mathbf{m}_{\text{Fe}}^2 = -\mathbf{m}_{\text{Fe}}^3 = \mathbf{m}_{\text{Fe}}^4, \quad (\text{A6})$$

and the internal hyperfine field on the  $^{77}\text{Se}$  site is derived as

$$\mathbf{H}_{in} = 4A_{hf}^{ab} \begin{bmatrix} m_{Fe}^b \\ m_{Fe}^a \\ 0 \end{bmatrix}. \quad (\text{A7})$$

Therefore, the stripe- and the checkerboard-type antiferromagnetic orders produce different hyperfine fields on  $^{77}\text{Se}$ , providing a method to differentiate two types of orders.

The stripe- and checkerboard-type spin fluctuations also lead to different anisotropy of the  $1/^{77}\text{T}_1$  for fields applied along different crystal directions. Following the same procedure as done in FeAs materials<sup>2</sup>, the  $1/^{77}\text{T}_1$  with different field orientations are obtained as

$$\begin{bmatrix} \left(\frac{1}{T_1}\right)_{H \parallel a} \\ \left(\frac{1}{T_1}\right)_{H \parallel b} \\ \left(\frac{1}{T_1}\right)_{H \parallel c} \end{bmatrix} \propto \begin{bmatrix} \langle A_{hf}^{ac} m_{Fe}^a(\omega_{res}) \rangle^2 \\ \langle m_{Fe}^a(\omega_{res}) \rangle^2 + \langle A_{hf}^{ac} m_{Fe}^c(\omega_{res}) \rangle^2 \\ \langle A_{hf}^{ac} m_{Fe}^c(\omega_{res}) \rangle^2 \end{bmatrix} \quad (\text{A8})$$

for the stripe-type spin fluctuations. On the other hand, the checkerboard-type fluctuations give

$$\begin{bmatrix} \left(\frac{1}{T_1}\right)_{H \parallel a} \\ \left(\frac{1}{T_1}\right)_{H \parallel b} \\ \left(\frac{1}{T_1}\right)_{H \parallel c} \end{bmatrix} \propto \begin{bmatrix} \langle A_{hf}^{ab} m_{Fe}^a(\omega_{res}) \rangle^2 \\ \langle A_{hf}^{ab} m_{Fe}^b(\omega_{res}) \rangle^2 \\ \langle A_{hf}^{ab} m_{Fe}^a(\omega_{res}) \rangle^2 + \langle A_{hf}^{ab} m_{Fe}^b(\omega_{res}) \rangle^2 \end{bmatrix}. \quad (\text{A9})$$

At high temperatures with only short-range magnetic correlations, it is reasonable to assume  $\langle m_{Fe}^a(\omega_{res}) \rangle^2 = \langle m_{Fe}^b(\omega_{res}) \rangle^2 = \langle m_{Fe}^c(\omega_{res}) \rangle^2$ . Taking  $(1/T_1)_{H \parallel a\&b} = [(1/T_1)_{H \parallel a} + (1/T_1)_{H \parallel b}]/2$ , we get the anisotropy factor  $R = (1/T_1)_{H \parallel a\&b}/(1/T_1)_{H \parallel c}$ .  $R = 1.5$  for the stripe-type fluctuations and 0.5 for the checkerboard-type fluctuations.

### S5. $^{77}\text{Se}$ NMR lineshapes for the locked, partially unlocked and fully unlocked stripe antiferromagnetic order

Following S4, if the Fe moments orientates along the  $a$ -axis of the orthorhombic structure, locked by the spin-orbit coupling, the hyperfine field on the  $^{77}\text{Se}$  nucleus is reduced to  $\mathbf{H}_{in} =$



$4A_{hf}^{ac}(0, 0, \pm m_{Fe}^a)$ . Then the NMR spectra under external fields have a single peak with  $H \parallel a&b$ , and double peaks with  $H \parallel c$ , as demonstrated in Fe pnictides1 and the simulated spectra shown in Fig. S5a.

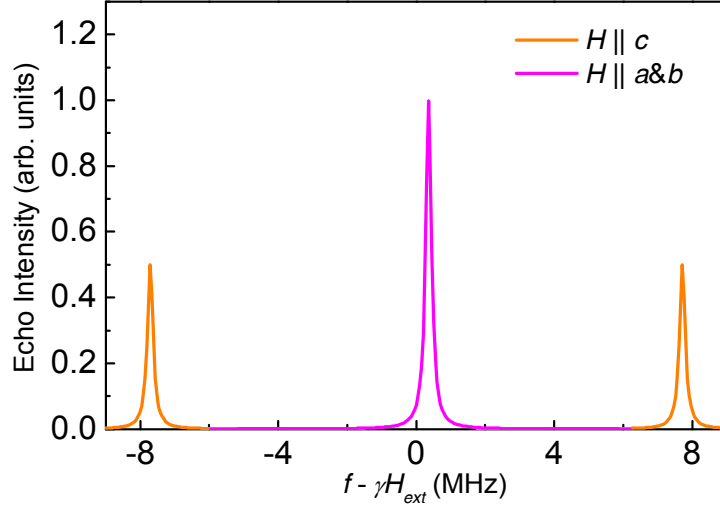


**Figure S5a.** The simulated  $^{77}\text{Se}$  NMR spectra with parameters  $H_{ext} = 10.3$  T and  $H_{in}^c = 0.95$  T for the stripe-order with the Fe moments locked along the  $a$ -axis of crystal.

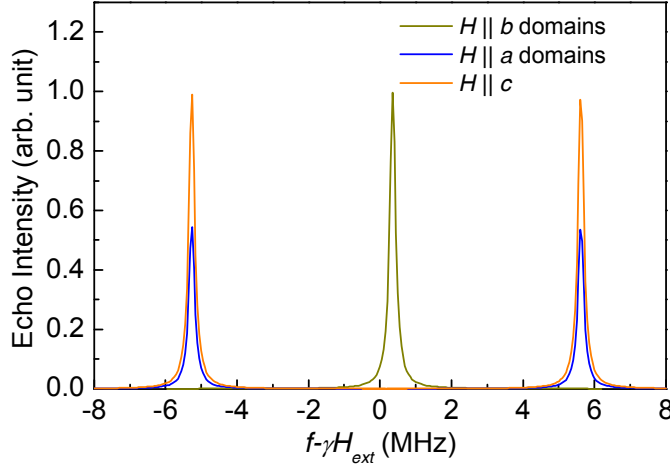


**Figure S5b.** The simulated  $^{77}\text{Se}$  NMR spectra with parameters  $H_{ext} = 10.3$  T and  $H_{in}^a = H_{in}^c = 0.672$  T ( $H_{in}^{total} = \sqrt{(H_{in}^a)^2 + (H_{in}^c)^2} = 0.95$  T) for the partially unlocked stripe-order antiferromagnetism.

For the partially unlocked stripe order, the Fe moments distribute around a direction with nonzero  $a$  and  $c$  components. This causes an eight-fold degeneracy with  $(\pm m_{Fe}^a, \pm m_{Fe}^b, \pm m_{Fe}^c)$  in the antiferromagnetic state. According to **S4**, the hyperfine fields on the  $^{77}\text{Se}$  nuclei have both  $a$  and  $c$  components with  $(H_{in}^a, H_{in}^b, H_{in}^c) = A_{hf}^{ac}(\pm m_{Fe}^c, 0, \pm m_{Fe}^a)$ . For  $H \parallel b$ , the  $^{77}\text{Se}$  spectrum shifts to a

slightly higher frequency upon ordering, because the internal field is orthogonal to the external field.

With  $H \parallel a$  or  $c$ , the single-peak spectra splits into two lines, with frequency separation  $\sim 2\gamma A_{hf}^{ac} m_{Fe}^c$

and  $2\gamma A_{hf}^{ac} m_{Fe}^a$ , respectively. In this case, sharp NMR lines should be observed as shown in Fig. S5b.

For the fully unlocked case, the ordered Fe moments are written as,

$$\mathbf{m} = m \begin{bmatrix} \sin \theta \cos \phi \\ \sin \theta \sin \phi \\ \cos \theta \end{bmatrix},$$

where  $\theta$  is the angle between the  $c$ -axis and the Fe moment, and  $\phi$  is the angle between the  $a$ -axis and

the projected Fe moment in the  $ab$ -plane. Then the hyperfine field on  $^{77}\text{Se}$  nucleus is,

$$\mathbf{H}_{\text{Se}} = A_{hf}^{ac} \begin{bmatrix} m \cos \theta \\ 0 \\ m \sin \theta \cos \phi \end{bmatrix}.$$

For convenience, we set  $H_{in} = A_{hf}^{ac} m$ . The field can be written as  $\mathbf{H}_{\text{Se}} = H_{in} \begin{bmatrix} \cos \theta \\ 0 \\ \sin \theta \cos \phi \end{bmatrix}$ .

Then we introduce an applied NMR field,

$$\mathbf{H}_o = H_{ext} \begin{bmatrix} \sin \alpha \cos \beta \\ \sin \alpha \sin \beta \\ \cos \alpha \end{bmatrix},$$

where  $\alpha$  is the angle between the  $c$ -axis and the external field and  $\beta$  is angle between the  $a$ -axis and the

projected external field in the  $ab$ -plane. The total field on the  $^{77}\text{Se}$  nucleus is written as,

$$\mathbf{H}_{total} = \begin{bmatrix} H_{in} \cos \theta + H_{ext} \sin \alpha \cos \beta \\ H_{ext} \sin \alpha \sin \beta \\ H_{in} \sin \theta \cos \phi + H_{ext} \cos \alpha \end{bmatrix}.$$

By approximation,  $H_{total}$  can be further written as

$$H_{total} = H_{ext} + H_{in} (\cos \theta \sin \alpha \cos \beta + \sin \theta \cos \phi \cos \alpha).$$

In Fig. S5c, the simulated spectra are shown under three field configurations. With  $H \parallel b$ , the spectrum is sharply peaked. For  $H \parallel a$  or  $c$ , the spectrum is flat and broadly distributes between  $-\gamma H_{in}$

and  $+\gamma H_{in}$ . For other field directions, the spectra are also nearly flat and distribute approximately between  $-\gamma H_{in} \sin \delta$  and  $+\gamma H_{in} \sin \delta$  with the echo intensity proportional to  $1/\sin \delta$ , where  $\delta$  is the angle between the external field and the  $b$ -axis.

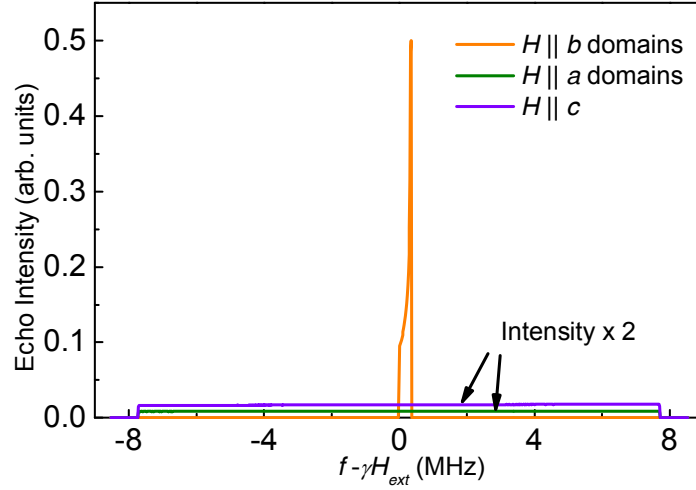


**Figure S5c.** The simulated NMR spectra with parameters  $H_{ext} = 10.3$  T and  $H_{in} = 0.95$  T in the fully unlocked stripe order phase with  $H \parallel a\&b$  and  $H \parallel c$ .

### S6. Lineshape analysis on the measured $^{77}\text{Se}$ NMR spectra at $P = 2.4$ GPa

As shown in the main text with  $H \parallel a\&b$ , the observed spectra have only one peak at  $\sim 83.7$  MHz with 50% spectral weight loss. Among the three simulated spectra shown in Fig. S5a-c, only the uS-AFM one is compatible with the experimental results.

With similar analysis, our data rule out the following proposed magnetic orders:

- (i) Spin glass. All our spin-lattice relaxation follows perfect single exponential recovery with no signal wipeout, ruling out any spin glass phase.
- (ii) Commensurate or incommensurate stripe-order AFM with Fe moments locked in the  $ab$ -plane. This would lead to 100% remaining spectra weight below  $T_N$  with  $H \parallel a\&b$ .

- (iii) Stripe-order AFM with Fe moments locked along the  $c$ -axis. This would lead to a non-split NMR line with 100% weight below  $T_N$  with  $H \parallel c$ .
- (iv) Checkerboard-type spin fluctuations and magnetic order. In the checkerboard-type order, the neighboring Fe moments are aligned antiferromagnetically along both  $a$ - and  $b$ -axis of crystal. As shown in S4, the checkerboard-type fluctuations would give an anisotropy factor  $R = 0.5$ . This is clearly different from our data (Fig. 3d of the main text). The  $^{77}\text{Se}$  hyperfine field with the checkerboard-type order is calculated to be  $(H_{in}^a, H_{in}^b, H_{in}^c) = (A_{hf}^{ab}m_{Fe}^b, A_{hf}^{ab}m_{Fe}^a, 0)$ . Therefore, no spectral weight loss is expected with  $H \parallel c$ , in contradiction to our data (Fig. 3a of the main text). The checkerboard-type  $(\pi, \pi)$  fluctuations, revealed by inelastic neutron scattering at the ambient pressure<sup>3</sup>, seem not essential for FeSe at high pressures.
- (v) Mixture of local checkerboard and stripe patterns, such as double-stripe, staggered dimer, and staggered trimer orders<sup>4,5</sup>. This would lead to a large spectral weight close to the central frequency with  $H \parallel c$  below  $T_N$ .
- (vi) Incommensurate SDW or spiral order with a propagating wave vector far away from  $(\pi, 0)$  or  $(0, \pi)$ . This would lead to different anisotropy factor in  $1/T_1$  above  $T_N$  and much less spectral weight close to the central frequency with  $H \parallel a \& b$  below  $T_N$ .

## References

1. Kitagawa, K., Katayama, N., Ohgushi, K., Yoshida, M. & Takigawa, M. Commensurate Itinerant Antiferromagnetism in  $\text{BaFe}_2\text{As}_2$ :  $^{75}\text{As}$ -NMR Studies on a Self-Flux Grown Single Crystal. *J. Phys.*

- Soc. Jpn.* **77**, 114709 (2008).
2. Kitagawa, S. *et al.* Stripe antiferromagnetic correlations in  $\text{LaFeAsO}_{1-x}\text{F}_x$  probed by  $^{75}\text{As}$  NMR. *Phys. Rev. B* **81**, 212502 (2011).
  3. Wang, Q. S. *et al.* Magnetic ground state of FeSe. Preprint at <http://arxiv.org/abs/1511.02485> (2015).
  4. Glasbrenner, J. K., Mazin, I. I., Jeschke, H. O., Hirschfeld, P. J., Fernandes R. M. & Valentí, R. Effect of magnetic frustration on nematicity and superconductivity in iron chalcogenides. *Nature Phys.* **11**, 953-958 (2015).
  5. Liu, K., Lu, Z-Y & Xiang, T. Nematic antiferromagnetic states in bulk FeSe. Preprint at <http://arxiv.org/abs/1510.07447> (2015).